Decoherence in a spin–spin-bath model with environmental self-interaction

2003 J. Phys. A: Math. Gen. 36 12305

(http://iopscience.iop.org/0305-4470/36/49/012)

INSTITUTE OF PHYSICS PUBLISHING JOURNAL OF PHYSICS A: MATHEMATICAL AND GENERAL

J. Phys. A: Math. Gen. **36** (2003) 12305–12327 PII: S0305-4470(03)62110-4

Decoherence in a spin–spin-bath model with environmental self-interaction

L Tessieri[1] **and J Wilkie**

Department of Chemistry, Simon Fraser University, Burnaby, British Columbia V5A 1S6, Canada

Received 9 April 2003
Published 25 November 2003
Online at stacks.iop.org/JPhysA/36/12305

Abstract

A low-temperature model system consisting of a central spin coupled to a spin-bath is studied to determine whether interaction among bath spins has an effect on central spin dynamics. In the absence of intra-environmental coupling, decoherence of the central spin is fast and irreversible. Strong intra-environmental interaction results in an effective decoupling of the central spin from the bath and suppression of decoherence. Weaker intra-environmental coupling reduces but does not eliminate decoherence. We argue that similar suppression of decoherence should be observed for electronic states of He impurities in silicon or diamond.

PACS number: 03.65.Yz

1. Introduction

Exact theories for the dynamics of open quantum systems require solution of the Schrödinger equation (or an equivalent formalism) for the full system plus environment degrees of freedom. This is impossible to do analytically except when the environment consists of a set of independent harmonic oscillators (e.g., Caldeira–Leggett model [1], spin-boson model [2], Haake–Reibold model [3]) or spins [4]. Neglect of intra-environmental coupling is thus strongly motivated by reasons of mathematical convenience. For some interactions, such as with nuclear spins of impurities in a solid at low temperature, the approximation seems justified [4]. For general interactions the importance of bath self-interaction is less clear. (See for example the conflicting opinions expressed in [5, 6].) The purpose of the present study is to determine what effect intra-environmental coupling has on subsystem dynamics. We thus consider the strength of bath self-interaction as a parameter in an idealized model which does not represent any particular physical environment. To make exact numerical calculations possible we chose a model system consisting of a small (i.e., highly quantum) central spin interacting with a bath of self-interacting spins representing the degrees of freedom of the environment. We shall sometimes refer to this central spin as the subsystem.

[1] Present address: Instituto de Física Matemáticas, Universidad Michoacana de San Nicolás de Hidalgo, 58060 Morelia, Michoacán, Mexico.

0305-4470/03/4912305+23$30.00

Intuition suggests that coupling between environment degrees of freedom can significantly affect the properties of the bath and consequently, through subsystem-environment coupling, the dynamics of the central spin. Mutual interactions of the bath modes allow energy exchange without using the subsystem as an intermediary. Consider an initial state of the subsystem-environment which is perturbed away from equilibrium. With intra-environmental coupling the rapid initial flow of energy towards a new equilibrium state will largely occur within the environment. Without intra-environmental coupling the energy must flow through the subsystem, leaving it strongly entangled with the bath and hence badly decohered. (Note that the decoherence effects discussed in this manuscript differ greatly from those which affect macroscopic subsystems [7].)

Intra-environmental interactions may also alter more abstract properties of the bath. The classical dynamics of a bath of oscillators can change from regular to chaotic when nonlinear interactions are added [8]. In the quantum case, such coupling modifies the statistical properties of the energy levels and eigenstates of the bath. Specifically, the energy spectra of quantum systems with chaotic classical counterpart exhibit level repulsion, while systems with regular dynamics in the classical limit show a clustering of the energy levels [9] and high degeneracy. The structure of the bath eigenstates also changes when the dynamics of the bath undergoes a transition from regular to chaotic. This effect can be analysed by considering the form of the Wigner functions of energy eigenstates: for chaotic systems the Wigner functions spread more or less uniformly over the energetically available phase space [10], whereas in the case of regular systems they are more lumpy. Moreover, these spectral signatures of chaos have dynamical consequences [11]. It is therefore reasonable to expect that dissipation and decoherence will assume different forms for coupled and uncoupled baths.

Experimental evidence for the presence of microscopic chaos in fluid systems has recently been obtained for Brownian motion of a colloidal particle in water [12]. Numerical evidence for chaos in the solid state has been obtained via molecular dynamics calculations of nuclear motions in silicon crystals [13], and for the electronic band structures of silicon [14]. Propagation of acoustic phonons in Si crystals is also known to be highly sensitive to anharmonic phonon–phonon interaction [15]. Thus, there is growing evidence for the presence of microscopic chaos in the sort of macroscopic thermodynamic systems which in decoherence studies are customarily modelled as baths of non-interacting oscillators or spins.

A qualitative understanding of the effects of bath self-interaction on decoherence, while of obvious theoretical interest, might also have important applications. Minimization of decoherence is essential for the development and implementation of a number of new technologies such as quantum computing [16], laser control of chemical reactions [17] and molecular electronics [18]. For quantum computing some proposed physical platforms, such as laser manipulated cold ions in traps in near vacuum [19, 20] can very effectively minimize decoherence. Whether such platforms can be scaled to the 10^5 ions needed to perform useful computations like factorization of large integers is unclear [20]. Proposed solid state platforms such as single-electron quantum dots embedded in a semiconductor [21] are readily scalable [22], but decoherence is a serious obstacle. In principle, the effects of decoherence and dissipation can be reduced through judicious choice of states for implementation of the qubit [23] (a trivial example would be to avoid states with electric-dipole allowed transitions) and through error correction codes [16]. Since the solid state in principle provides enormous freedom over the choice of qubit and matrix, further theoretical insight into the mechanisms of decoherence might prove extremely useful in selecting optimal configurations.

The effect of environmental self-interaction is almost certainly of importance in the solid state. Unfortunately, as we noted above, the analysis of the mechanisms of decoherence and dissipation in self-interacting environments is a problem that defies exact analytical

treatments. Standard approaches, such as the Feynman–Vernon influence functional method [24] or the Nakajima–Zwanzig projection technique [25] cannot be successfully applied unless restrictive hypotheses are made on the nature of the bath and its coupling to the subsystem of interest. Thus, for exact results we must rely on what we can calculate numerically. Environments with few degrees of freedom should in principle provide much of the qualitative information we seek. Such numerical studies also serve a second purpose, namely to provide exact results which can be used as a touchstone to test the reliability of the approximate analytical methods which describe open systems (e.g., master equation obtained using the Redfield [26] or the stochastic resonance approximation [27] and other approaches [28]).

Because we must treat intra-environmental coupling as a parameter, the spin–spin-bath model employed here does not map directly onto any particular physical system. We choose near resonant subsystem and bath frequencies, and strong subsystem-environment coupling, so that decoherence is strong in the absence of intra-environmental coupling. We show that decoherence is greatly reduced as the intra-environmental coupling increases. We argue that this is a consequence of a transition from integrable to chaotic bath dynamics and that similar effects will be observed in more general environments.

In the specific case of strong intra-environmental coupling our model could be experimentally implemented as an interstitial He in an otherwise pure silicon or diamond [29] cluster. The subsystem (qubit) consists of the ground and one excited electronic state of He of the same parity. Electric dipole matrix elements thus vanish and optical transitions can be neglected. The primary mechanism of decoherence and dissipation is thus vibronic coupling of He with phonons of the cluster. We imagine the cluster as a finite model of a macroscopic crystal. For example, the band gap of Si is well reproduced in a cluster of only 26 atoms [30]. A detailed discussion of He-(silicon, diamond) as a potential platform for quantum computing will be presented elsewhere. Here we focus on decoherence of a single qubit. Since He is known to cause small lattice distortion [31] the crystal vibrational Hamiltonians corresponding to the ground and excited states of He are taken to be identical. As a result the vibronic Hamiltonian of the impurity and crystal takes the form

$$H = \frac{\hbar\omega_0}{2}\sigma_z^{(0)} + \sigma_y^{(0)}\sum_{k=1}^{N}(\alpha_k P_k + P_k\alpha_k) + \sigma_x^{(0)}\Lambda_0 + 1^{(0)}(T_n + V(Q)) \tag{1}$$

where $\sigma_i^{(0)}$ (with $i = x, y, z$) denote the Pauli matrices representing the state of the impurity, P and Q denote phonon momenta and coordinates, and $T_n = \sum_{k=1}^{N} P_k^2/2M_n$ and $V(Q)$ are the nuclear kinetic and potential energies. The potential $V(Q)$ includes anharmonic phonon–phonon interactions which are known from experiment to be strong in silicon and diamond [32]. Finally,

$$\alpha_k(Q) = \frac{\hbar}{2M_n}\left\langle\phi_1\left|\frac{\partial\phi_2}{\partial Q_k}\right.\right\rangle \qquad \Lambda_0(Q) = \frac{\hbar^2}{2M_n}\sum_{k=1}^{N}\left\langle\frac{\partial\phi_1}{\partial Q_k}\left|\frac{\partial\phi_2}{\partial Q_k}\right.\right\rangle \tag{2}$$

are the small (i.e., $O(m_e/M_n) \sim 10^{-4}$) vibronic couplings arising from the nuclear coordinate dependence of the confined He electronic wavefunctions ϕ_1 and ϕ_2.

Quantum dynamical simulation of more than a few coupled oscillators is currently impossible because computational costs scale exponentially with the number of modes. To simulate qubit dynamics under Hamiltonian (1) it is therefore necessary to truncate the number of allowed excitations per phonon mode and restrict the number of participating phonon modes. Provided that these limitations do not alter the chaotic character of the phonon dynamics we expect qualitatively similar decoherence from this more idealized model. The fact that integers are stored in binary form in computer memory strongly favours representation of the phonons

as two state (i.e., spin-1/2) systems. The resulting spin–spin-bath model differs from those previously studied where intra-environmental coupling has either been neglected completely [33] or included only in a mean-field sense [4, 34]. Assuming a Debye (i.e. quadratic) distribution of the frequencies for the phonon modes, the high Debye temperatures of silicon (645 K) and diamond (1860 K) imply that most will be frozen in their ground states at liquid nitrogen temperatures (77 K). Frequencies should thus be sampled below an effective frequency cutoff ω_c determined by the relevant temperature. Most sampled modes will have frequencies near ω_c because of the quadratically increasing nature of the spectrum. The low-frequency modes which we thus neglect are much smaller than the impurity frequency ω_0, are hence non-resonant, and are not expected to play an important role.

Using this model we show that environmental self-interaction has an extremely important effect on decoherence. Strong intra-environmental interactions effectively decouple the subsystem from the environment, and even weak interactions qualitatively change the manner in which phase information is lost. In section 5 we present a general semi-classical argument that similar effects will be observed in the true Hamiltonian (1).

Section 2 explains our model in detail. In section 3 we outline the numerical methods we employ to solve the subsystem dynamics. Numerical results for subsystem dynamics are discussed in detail in section 4 for a wide range of intra-environmental couplings. We summarize our findings for the spin–spin-bath in section 5 and show that similar results should hold for the true vibronic Hamiltonian (1).

2. The spin–spin-bath model

Representing the phonons of Hamiltonian (1) by spin-1/2 modes results in simplifications such as

$$\frac{P_k^2}{2M_n} + \frac{M_n\omega_k^2}{2}Q_k^2 \to \frac{\hbar\omega_k}{2}\sigma_z^{(k)} \qquad Q_k \to \sigma_x^{(k)} \qquad P_k \to \sigma_y^{(k)} \qquad Q_j Q_k^3 \to \sigma_x^{(j)}\sigma_x^{(k)}$$

which, once the terms (2) are expanded to the first order in powers of Q, lead to the vanishing of the momentum coupling terms in (1) as a result of the fact that σ_x and σ_y anti-commute.

As a consequence of these simplifications, we can replace the solid-state model (1) with the spin system defined by the Hamiltonian

$$H = H_0 + H_B + H_I \tag{3}$$

where

$$H_0 = \frac{\hbar\omega_0}{2}\sigma_z^{(0)} + \beta\sigma_x^{(0)} \tag{4}$$

is the Hamiltonian of the central spin (denoted by the superscript 0),

$$H_B = \sum_{i=1}^{N}\frac{\hbar\omega_i}{2}\sigma_z^{(i)} + \beta\sum_{i=1}^{N}\sigma_x^{(i)} + \lambda\sum_{i=1}^{N-1}\sum_{j=i+1}^{N}\sigma_x^{(i)}\sigma_x^{(j)} \tag{5}$$

is the Hamiltonian of the bath, and

$$H_I = \lambda_0\sum_{i=1}^{N}\sigma_x^{(i)}\sigma_x^{(0)} \tag{6}$$

describes the interaction between the central spin and its environment. For simplicity, in the rest of this paper we adopt a system of units such that $\hbar = 1$. Note that the terms proportional to β and λ in Hamiltonians (4) and (5) represent nonlinear spin interactions in the spin model

(3) but can be interpreted as anharmonic phonon–phonon interactions if one considers the Hamiltonian (3) as a low-temperature approximation for the model (1).

To complete the definition of the model, we have to specify the values of the various parameters which appear in the Hamiltonian. We assume that the frequencies of the bath spins are positive random variables with the Debye probability density

$$p(\omega) = \begin{cases} 3\omega^2/\omega_c^3 & \text{for} \quad 0 < \omega < \omega_c \\ 0 & \text{for} \quad \omega_c < \omega \end{cases} \tag{7}$$

appropriate for the low-energy acoustic modes of a crystal. The cut-off frequency ω_c need not be the Debye frequency ω_D; in fact, at the low temperatures we consider, modes with large frequency are unlikely to be populated and so it makes sense to choose ω_c smaller than ω_D to reflect this fact. For the frequency of the central spin, we arbitrarily chose the value $\omega_0 = 0.8288\omega_c$. Note that the results obtained in this manuscript do not depend crucially on the specific form (7) of the frequency distribution. In fact, we repeated our calculations with the box distribution

$$p(\omega) = \begin{cases} 1/\omega_c & \text{for} \quad 0 < \omega < \omega_c \\ 0 & \text{for} \quad \omega_c < \omega \end{cases}$$

(which more heavily weights small frequencies) and found the qualitative behaviour of the model unaltered by the change.

To simplify the form of mathematical expressions, we set $\omega_c = 1$, $\lambda_0 = 1$, and we varied the relative strength of the intra-environmental interactions by letting the parameter λ range in the interval from $\lambda = 0$ (bath without internal spin–spin coupling) to $\lambda = 10$ (strong bath self-interaction). In addition to considering positive values of λ, which correspond to antiferromagnetic interactions, we investigated the case of ferromagnetic couplings, letting λ assume negative values in the interval $[-10, 0]$.

We set $\beta = 0.01$. An important consequence of the fact that β, although small, is not zero, is that the Hamiltonian (3) cannot be reduced to block form. To understand this point, we observe that the Hilbert space of the system (3) is spanned by the vectors

$$\begin{aligned} |0\rangle &= |0\rangle_N |0\rangle_{N-1} \dots |0\rangle_1 |0\rangle_0 \\ |1\rangle &= |0\rangle_N |0\rangle_{N-1} \dots |0\rangle_1 |1\rangle_0 \\ |2\rangle &= |0\rangle_N |0\rangle_{N-1} \dots |1\rangle_1 |0\rangle_0 \\ &\vdots \\ |2^{N+1} - 1\rangle &= |1\rangle_N |1\rangle_{N-1} \dots |1\rangle_1 |1\rangle_0 \end{aligned} \tag{8}$$

where the symbols $|1\rangle_i$ and $|0\rangle_i$ denote the 'up' and 'down' states of the ith spin, i.e., the eigenstates of the Pauli z-spin matrix $\sigma_z^{(i)}$ with eigenvalues $+1$ and -1 respectively. Note that the basis states (8) can be conveniently interpreted as binary representations of integer numbers ranging from 0 to $2^{N+1} - 1$ if the vector

$$|k_N, k_{N-1}, \dots, k_0\rangle = |k_N\rangle_N |k_{N-1}\rangle_{N-1} \dots |k_0\rangle_0 \tag{9}$$

(with $k_i = 0, 1$ for $i = 0, \dots, N$) is associated with the integer

$$k = k_0 + 2k_1 + \dots + 2^N k_N = \sum_{n=0}^{N} 2^n k_n. \tag{10}$$

For $\beta = 0$ the Hamiltonian (3) can be reduced to block form by regrouping the basis vectors (8) in two sets defined by the condition that the states of each set have an even or odd number

of spins 'up'. In fact, for $\beta = 0$ all terms of the Hamiltonian (3) have the effect of flipping either zero or two spins at once, thereby leaving invariant the subspaces spanned by the 'even' and 'odd' basis states. The terms proportional to β, on the other hand, flip just one spin and therefore connect the 'even' and 'odd' subspaces, making the Hamiltonian (3) irreducible.

3. Numerical approach

Assume that the bath is initially in thermal equilibrium at temperature T and that the central spin is in the excited state $|1\rangle_0$. (In the case of an impurity in a insulating solid such an initial state could be prepared using a fast laser pulse with a frequency matching a transition of the impurity but lying in the crystal's band gap.) The initial density matrix of the whole system therefore has the product form

$$\rho(0) = \rho_0(0) \otimes \rho_B(0) \tag{11}$$

with

$$\rho_0(0) = |1\rangle_{00}\langle 1| \qquad \text{and} \qquad \rho_B(0) = (1/Q)\exp(-H_B/kT)$$

where $Q = \mathrm{Tr}_B[\exp(-H_B/kT)]$. After introducing the notation

$$H_B\left|\phi_n^{(B)}\right\rangle = E_n\left|\phi_n^{(B)}\right\rangle \tag{12}$$

for the 2^N eigenvalues and eigenvectors of the bath Hamiltonian and

$$|\psi_n(0)\rangle = |1\rangle_0 \otimes \left|\phi_n^{(B)}\right\rangle \tag{13}$$

for the corresponding initial conditions of the total system, we can write the initial density matrix (11) in the form

$$\rho(0) = \sum_{n=1}^{2^N} |\psi_n(0)\rangle \frac{\mathrm{e}^{-E_n/kT}}{Q} \langle\psi_n(0)|.$$

To study the dynamics we have determined the states

$$|\psi_n(t)\rangle = \exp\left(-\mathrm{i}Ht\right)|\psi_n(0)\rangle \tag{14}$$

which evolve from (13). Once states (14) are known the evolved density is constructed via

$$\rho(t) = \exp(-\mathrm{i}Ht)\rho(0)\exp(\mathrm{i}Ht) = \sum_{n=1}^{2^N} |\psi_n(t)\rangle \frac{\mathrm{e}^{-E_n/kT}}{Q} \langle\psi_n(t)| \tag{15}$$

and the reduced density of interest is

$$\rho_0(t) = \mathrm{Tr}_B[\rho(t)] = \sum_{n,m} \left\langle\phi_m^{(B)}\middle|\psi_n(t)\right\rangle \frac{\mathrm{e}^{-E_n/kT}}{Q} \left\langle\psi_n(t)\middle|\phi_m^{(B)}\right\rangle. \tag{16}$$

We used two complementary techniques to compute the dynamics (14). For small baths, $N \leqslant 11$, we numerically diagonalized both the bath Hamiltonian (5) and the total Hamiltonian (3) using standard Householder routines (see [35]). This method gives the exact reduced density at all times and allows us to consider a range of temperature. However, it cannot be used for baths composed of a large number N of spins since matrices of size $2^N \times 2^N$ quickly exceed computer resources. For large baths with $N \geqslant 12$ spins, we exploited the low-temperature limit. For $kT \to 0$, high-energy eigenstates of the bath are depleted and one can truncate the sum in equation (15) to the first M terms, with $M \ll 2^N$, so that the density matrix takes the form

$$\rho(t) \simeq \sum_{n=1}^{M} |\psi_n(t)\rangle \frac{\mathrm{e}^{-E_n/kT}}{Q} \langle\psi_n(t)|. \tag{17}$$

Thus a complete diagonalization of the bath Hamiltonian becomes unnecessary. We chose a bath temperature of $kT = 0.02$ for which the number of terms M needed in (17) is 20. We checked that neglected terms were irrelevant by evaluating the probability that the bath be in an eigenstate of energy $E > E_{20}$. For baths with $N \leqslant 11$ spins with $0 \leqslant \lambda \leqslant 10$ we obtained an upper bound

$$P(E_B > E_{20}) = 1 - \sum_{n=1}^{20} \mathrm{e}^{-E_n/kT}/Q < 10^{-4}$$

showing that bath eigenstates with $E > E_{20}$ are unpopulated. As a further check, for baths composed of more than 11 spins we estimated the ratio $R = p_{20}/p_1 = \exp(E_1 - E_{20})$. For $N = 14$, $0 \leqslant \lambda \leqslant 10$ and $kT = 0.02$ the probability ratio was less than 10^{-6}.

To determine the M bath eigenstates of lowest energy, we used ARPACK routines based on the Lanczos algorithm[2]. Evolved states (14) were calculated using a Runge–Kutta algorithm of eighth order [36]. Neither the programmes for the partial diagonalization of the bath Hamiltonian, nor the Runge–Kutta subroutine required that the whole Hamiltonian matrix be stored in the computer memory, but only that the matrix-vector product $H|\psi\rangle$ be defined. This more efficient use of computer resources allowed us to consider baths of up to 14 spins.

We calculated $H|\psi\rangle$ given an input state $|\psi\rangle$ by iterated calls to subroutines which multiplied by $\sigma_x^{(i)}$ and $\sigma_z^{(i)}$. Consider multiplication by $\sigma_x^{(i)}$ as an example. With vectors (8) as a basis for our Hilbert space

$$\sigma_x^{(i)}|\psi\rangle = \sum_{k=0}^{2^{N+1}-1} \langle k|\psi\rangle \sigma_x^{(i)}|k\rangle \tag{18}$$

thus reducing our problem to that of finding an efficient way to multiply the basis vectors (8) by $\sigma_x^{(i)}$. Since the matrix $\sigma_x^{(i)}$ has the effect of flipping the ith spin, one has

$$\sigma_x^{(i)}|k_N, \ldots, k_i, \ldots, k_0\rangle = |k_N, \ldots, \overline{k_i}, \ldots, k_0\rangle$$

where $\overline{k_i} = 1$ if $k_i = 0$ and $\overline{k_i} = 0$ if $k_i = 1$. Multiplication by $\sigma_x^{(i)}$, therefore, replaces the kth component of $|\psi\rangle$ (where $k = k_0 + \cdots + 2^i k_i + \cdots + 2^N k_N$) with the k'th component (where $k' = k_0 + \cdots + 2^i \overline{k_i} + \cdots + 2^N k_N$) and vice versa. In binary representation, the numbers k and k' differ by a single bit (the ith bit) and one can therefore obtain k' from k using Fortran intrinsic functions. Specifically, we used the XOR-function (exclusive or) to flip the ith bit of the kth state. Multiplication by $\sigma_z^{(i)}$ can be similarly implemented.

After determining the evolved density (15), we traced out the bath degrees of freedom to obtain the reduced density (16). As indicators of quantum coherence, we chose the polarization and entropy of the central spin defined respectively as

$$\vec{P}(t) = \mathrm{Tr}[\rho_0(t)\vec{\sigma}] \tag{19}$$

and

$$S_0(t) = -\mathrm{Tr}\left[\rho_0(t) \ln \rho_0(t)\right] = -\frac{1}{2} \ln\left(\frac{1 - P^2}{4}\right) - \frac{P}{2} \ln\left(\frac{1 + P}{1 - P}\right). \tag{20}$$

Here $P = |\vec{P}|$ denotes the modulus of the polarization vector $\vec{P}$. Note that (19) contains as much information as the reduced density itself. In fact (16) can be expressed in terms of $\vec{P}$ via

$$\rho_0(t) = \tfrac{1}{2}(\mathbf{1} + \vec{P}(t) \cdot \vec{\sigma}).$$

[2] http://www.caam.rice.edu/software/ARPACK.

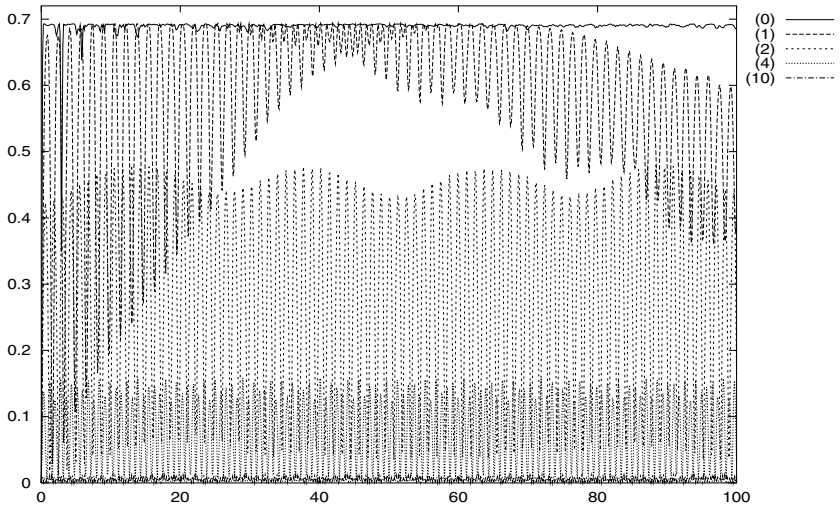

Figure 1. $S_0(t)$ versus $\omega_c t$ (14 bath spins).

4. Dynamics of the central spin

Here we examine the effects of intra-environmental couplings on the dynamics of the central spin. We consider the antiferromagnetic and the ferromagnetic cases separately. High-temperature results apply only to the case where the spin-bath represents true physical spins.

4.1. Antiferromagnetic interactions

To evaluate the effect of antiferromagnetic interactions we calculated the dynamics of the central spin for values of λ ranging from $\lambda = 0$ (uncoupled spins) to $\lambda = 10$ (strong coupling). As a point of reference, note that in the absence of *subsystem-environment* coupling $P_z(t)$—initially one—undergoes periodic fluctuations to slightly smaller values. The components $P_x(t)$ and $P_y(t)$—initially zero—oscillate about zero with the same period and similar small amplitude.

Entropy (20) is shown in figure 1. Figures 2–4 show components of the polarization (19). In the figures, each curve corresponds to a different value of the intra-environmental coupling λ (reported in parenthesis to the right). The thermal average was computed for a bath at temperature $kT = 0.02$. The results shown are for $N = 14$ but are also representative of smaller baths with even numbers of spins (i.e., 8, 10 and 12). The timescale considered is long enough for the system to attain its asymptotic condition as can be seen from figure 5 which shows the entropy of the central spin on a much longer timescale (data obtained for $N = 10$ spins).

When $\lambda = 0$ (i.e., bath spins non-interacting), the central spin undergoes rapid decoherence, with the polarization quickly falling to zero and the entropy $S_0(t)$ simultaneously approaching the maximum value $S_0^{\max} = \ln(2) \simeq 0.693\,147\ldots$. As λ increases, however, the entropy $S_0(t)$ tends to progressively smaller asymptotic values and the components of the polarization vector approach the dynamics of a central spin evolving in isolation. In other words, *the existence of a strong interaction among bath spins suppresses environmental decoherence*.

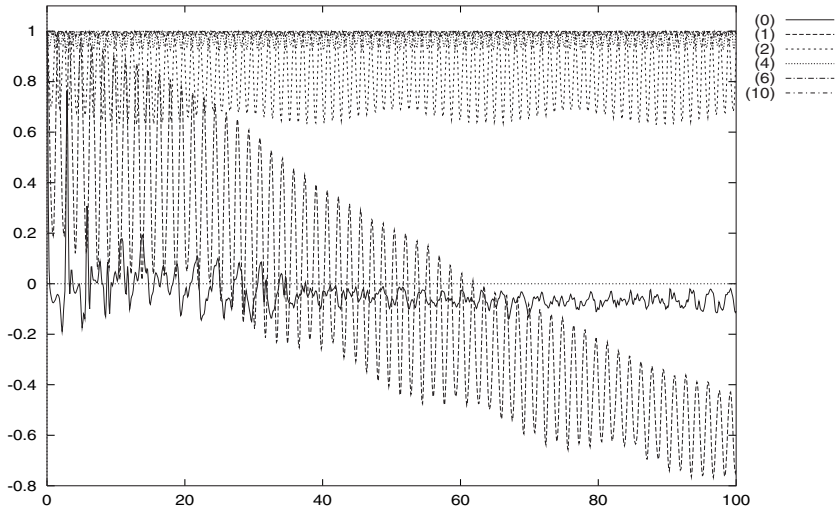

Figure 2. $P_z(t)$ versus $\omega_c t$ (14 bath spins).

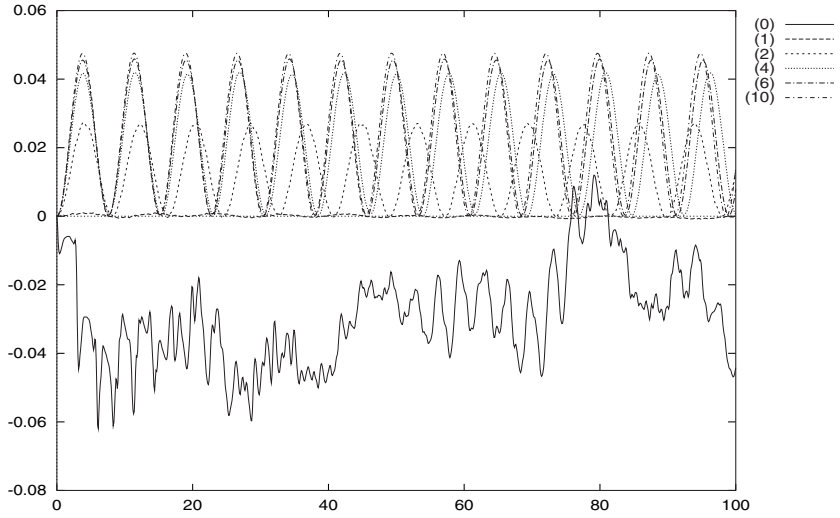

Figure 3. $P_x(t)$ versus $\omega_c t$ (14 bath spins).

This apparently puzzling result is a straightforward consequence of the fact that strong interactions between bath spins produce an almost complete decoupling of the central spin from the bath. This can be verified by considering the thermal average of the interaction Hamiltonian (6), defined as

$$\langle H_I(t)\rangle = \sum_{n=1}^{2^N} \langle\psi_n(t)|H_I|\psi_n(t)\rangle \, \mathrm{e}^{-E_n/kT}/Q. \tag{21}$$

Note that $\langle H_I(t)\rangle$, rather than λ_0, is the physically relevant quantity determining the strength of the interaction. In fact, the interaction may be small even if λ_0 is large. The evolution of $\langle H_I(t)\rangle$ is displayed in figure 6, which shows that as λ increases the effective interaction of the central spin with the bath tends to zero (data obtained for 10 spins). Quantitatively, $\langle H_I\rangle$

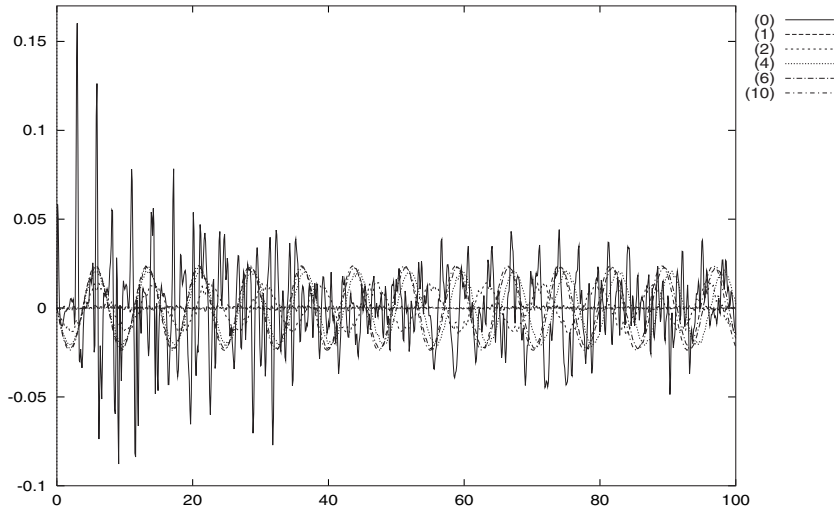

Figure 4. $P_y(t)$ versus $\omega_c t$ (14 bath spins).

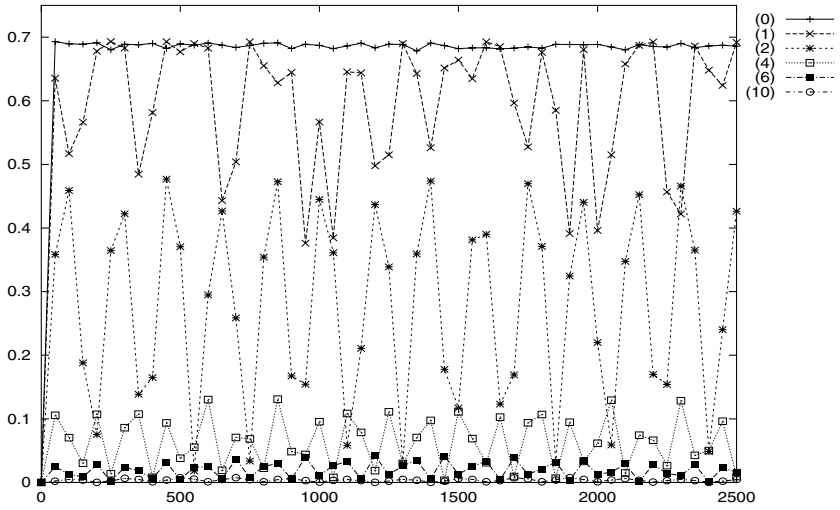

Figure 5. $S_0(t)$ versus $\omega_c t$ (10 bath spins).

averaged over the time interval $\left[0 : 2500\omega_c^{-1}\right]$ decreases from $\overline{\langle H_I \rangle} = -3.07$ for $\lambda = 0$ to $\overline{\langle H_I \rangle} = -0.01$ for $\lambda = 10$.

There is a simple explanation for the observed behaviour of the average interaction term (21). Define the total bath spin

$$\vec{\Sigma} = \sum_{i=1}^{N} \vec{\sigma}^{(i)} \tag{22}$$

(i.e., $\Sigma_x = \sum_{i=1}^{N} \sigma_x^{(i)}$, etc) and rewrite the interaction Hamiltonian (6) and bath Hamiltonian (5) in the suggestive forms

$$H_I = \lambda_0 \sigma_x^{(0)} \Sigma_x$$

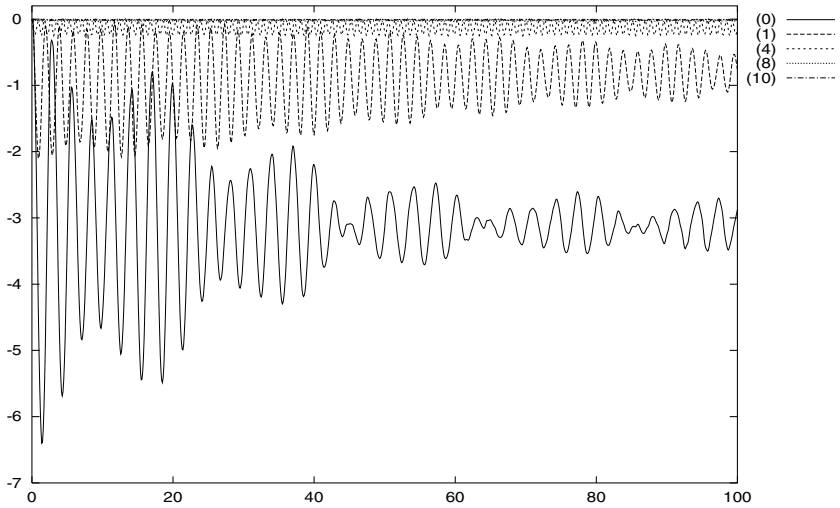

Figure 6. Thermal average $\langle H_I \rangle$ of the interaction Hamiltonian versus $\omega_c t$ (10 bath spins).

and

$$H_B = \frac{\lambda}{2}\left[\Sigma_x^2 - N\mathbf{1}\right] + \beta\Sigma_x + \sum_{i=1}^{N}\frac{\omega_i}{2}\sigma_z^{(i)}. \tag{23}$$

Equation (23) shows that for $\lambda \gg \omega_c$ the bath Hamiltonian takes the approximate form

$$H_B = \frac{\lambda}{2}\left[\Sigma_x^2 - N\mathbf{1}\right] + O(\lambda^0) \tag{24}$$

which is essentially proportional to Σ_x^2. Thus for large values of λ the bath eigenstates (12) must be approximate eigenvectors of Σ_x and those of lowest energy must correspond to the eigenstates of Σ_x with zero eigenvalue. (That many such eigenstates exist is a consequence of the fact for every value of the macroscopic variable Σ_x there are many corresponding microstates.) Thus, for low temperature and large λ the relevant diagonal and off-diagonal matrix elements of the environment coupling operator Σ_x will be zero.

These conclusions are confirmed by the numerical evaluation of the expectation values of Σ_x on the bath eigenstates (12). Figure 7 reports $\langle\phi_n^{(B)}|\Sigma_x|\phi_n^{(B)}\rangle$ as a function of the index n which orders the eigenstates $|\phi_n^{(B)}\rangle$ in ascending energy (data obtained for $N = 10$ so n runs from 1 to 1024). Data are shown for $\lambda = 0$ and $\lambda = 10$. For $\lambda = 0$ the expectation values of Σ_x are small but non-zero (this is more evident in the inset, which displays the data for the 100 lowest energies). For $\lambda = 10$ the expectation value of Σ_x has a sort of step-like behaviour and attains relatively large values for high-energy bath eigenstates. At low temperatures only low-energy states matter and for these $\langle\phi_n^{(B)}|\Sigma_x|\phi_n^{(B)}\rangle$ is orders of magnitude smaller than for the $\lambda = 0$ case (see inset in figure 7). This effect can be quantified by computing the quantity

$$\langle\Sigma_x\rangle = \frac{1}{20}\sum_{n=1}^{20}\langle\phi_n^{(B)}|\Sigma_x|\phi_n^{(B)}\rangle. \tag{25}$$

One finds

$$\langle\Sigma_x\rangle = \begin{cases} -0.161\,951 & \text{for} \quad \lambda = 0 \\ -6.0 \times 10^{-5} & \text{for} \quad \lambda = 10 \end{cases} \tag{26}$$

for $N = 10$ spins which is indeed small for strong coupling.

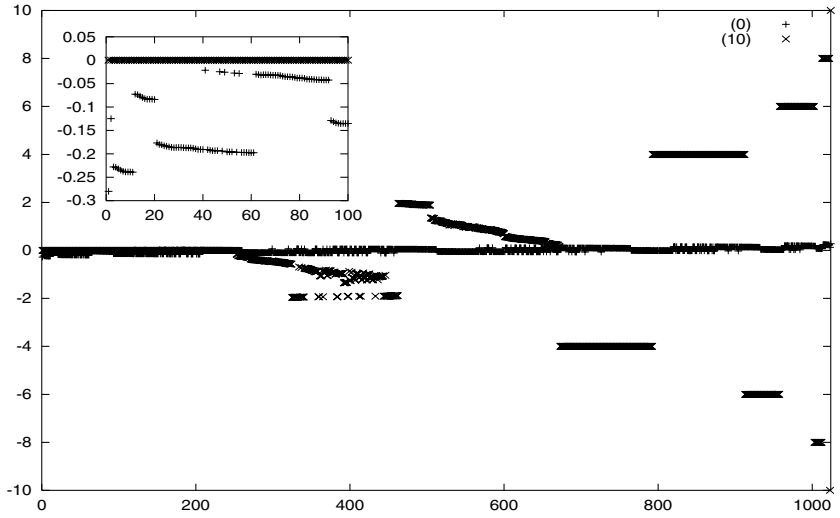

Figure 7. Expectation value $\langle\phi_n^{(B)}|\Sigma_x|\phi_n^{(B)}\rangle$ versus n for $\lambda = 0$ and $\lambda = 10$. The stacked inset shows on a larger scale the first 100 values. The data were obtained for a 10-spin bath.

The vanishing of the off-diagonal coupling matrix elements $\langle\phi_n^{(B)}|\Sigma_x|\phi_m^{(B)}\rangle$ is shown in figure 19 for $N = 14$ and $\lambda = 10$.

4.1.1. High-temperature limit. Figure 7, for $\lambda = 10$, shows that the expectation values of Σ_x are large for high-energy bath states. Populations in these states are zero at low temperatures but increase with temperature. The thermal average interaction (21) will therefore also increase with temperature, effectively coupling the central spin to its bath. As a consequence, one can expect that the self-interacting bath will behave more and more like an ordinary bath of uncoupled spins when the temperature is raised. Figure 8 shows the time behaviour of the central spin entropy for a bath of 10 coupled spins (with $\lambda = 10$) at various temperatures. Entropy increases monotonically with temperature, progressively approaching the behaviour characteristic of the uncoupled bath. However, even at high temperature ($kT = 300$) the entropy remains lower than for a bath of uncoupled spins: this shows that even at high temperatures the spin–spin coupling has a reductive effect on decoherence. These features are confirmed in figure 9. Raising the temperature lowers the asymptotic value of $P_z(t)$ which however never becomes zero.

In summary, at low temperatures the strong intra-environmental interactions force the bath spins to align in an antiferromagnetic state of zero moment and behave like a single giant spin decoupled from the central spin. As the temperature is raised thermal fluctuations eliminate the spin alignment and switch on the subsystem-environment coupling, making the self-interacting bath behave more like an ordinary bath of uncoupled spins.

4.1.2. Odd numbers of spins. So far we have considered the behaviour of a central spin coupled to a bath composed of an *even* number of spins. To complete the discussion of antiferromagnetic interactions, we briefly mention a last feature of the self-interacting spin bath—namely modifications which appear for baths with an *odd* number of spins.

Figures 10 and 11 show $S_0(t)$ and $P_z(t)$ for $N = 11$. Similar behaviour was obtained with baths of 5, 7 and 9 spins. Only $\lambda = 0, 1$ and 10 are shown because the curves for

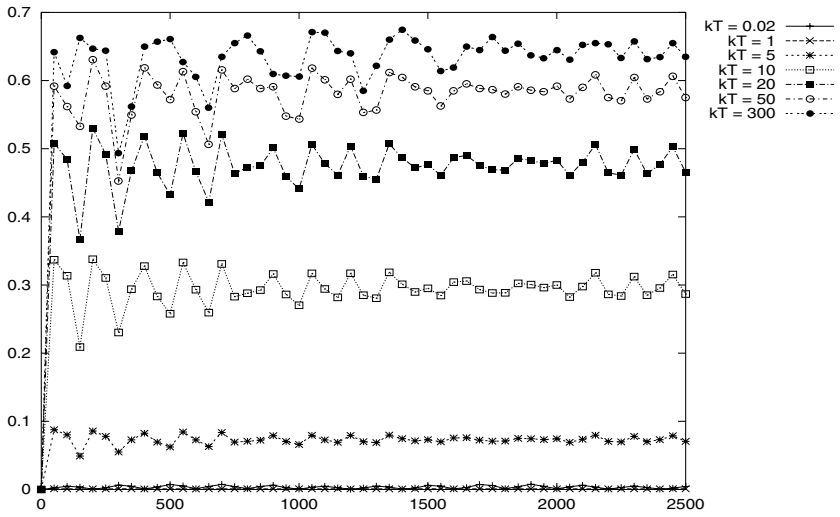

Figure 8. S_0 versus $\omega_c t$ for $\lambda = 10$ for various temperatures of the bath (10 bath spins).

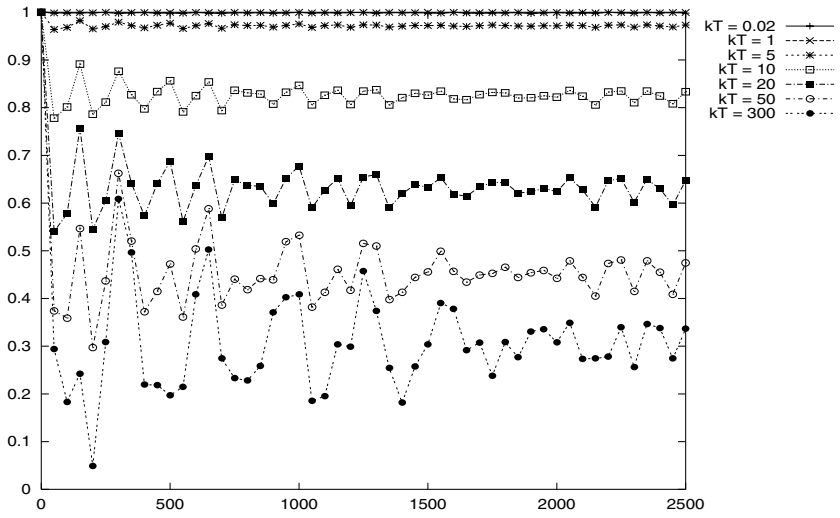

Figure 9. P_z versus $\omega_c t$ for $\lambda = 10$ for various temperatures of the bath (10 bath spins).

λ greater than 1 overlap. The data show that, regardless of whether the number of bath spins is even or odd, $S_0(t)$ is a decreasing function of the intra-environmental coupling. However, for N odd, the average value of the entropy decreases less than for N even and oscillates more (compare figures 10 and 1). Polarization behaves similarly. As shown in figure 11, when the intra-environmental interactions are strong, $P_z(t)$ oscillates around the value $P_z(t) \simeq 0.8$ for baths with odd number of spins, whereas one has $P_z(t) \simeq 1$ for a bath with an even number of spins. Nor do the oscillations die on a longer timescale: in fact, numerical calculations performed via the exact diagonalization of the Hamiltonian show oscillatory behaviour persisting on timescales an order of magnitude longer than that in figures 10 and 11. Thus intra-environmental interactions have the effect of suppressing

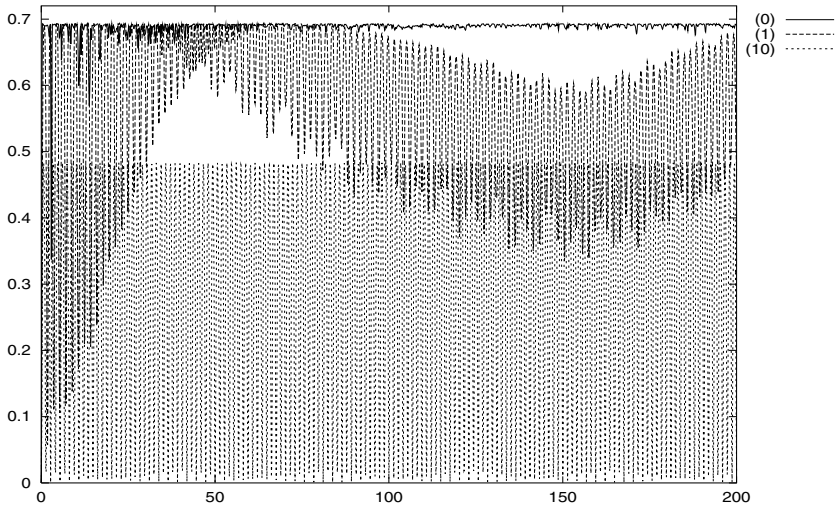

Figure 10. S_0 versus $\omega_c t$ (bath composed of 11 spins).

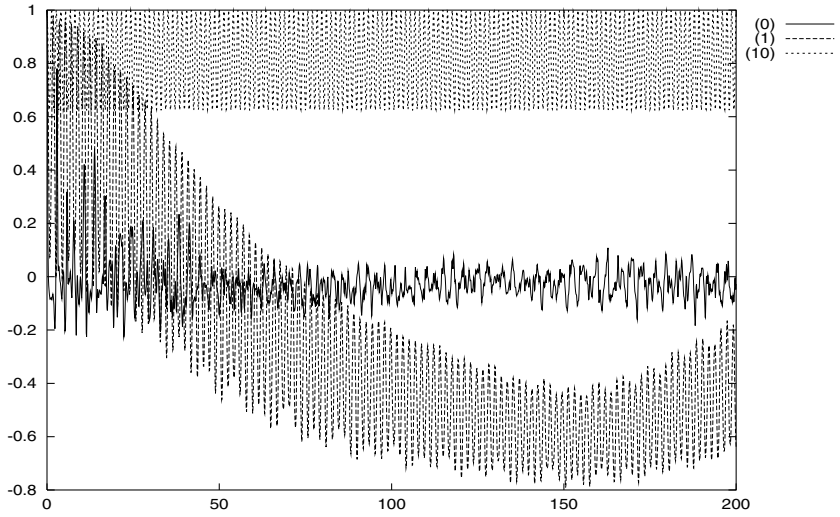

Figure 11. P_z versus $\omega_c t$ (bath composed of 11 spins).

decoherence regardless of how many spins compose the bath; however, this effect is more marked if the bath is composed of an even, rather than an odd, number of spins.

The oscillations of entropy and polarization are also displayed in the strength of the interaction between the central spin and its bath. Figure 12 shows the thermal average of the interaction Hamiltonian (6). Comparing figure 12 with figure 6, it is evident that the interaction between the central spin and bath is weaker for N even than N odd. Computing the parameter (25) for a bath of 11 spins gives

$$\langle \Sigma_x \rangle = \begin{cases} -0.191\,80 & \text{for} \quad \lambda = 0 \\ -4.97 \times 10^{-3} & \text{for} \quad \lambda = 10. \end{cases} \tag{27}$$

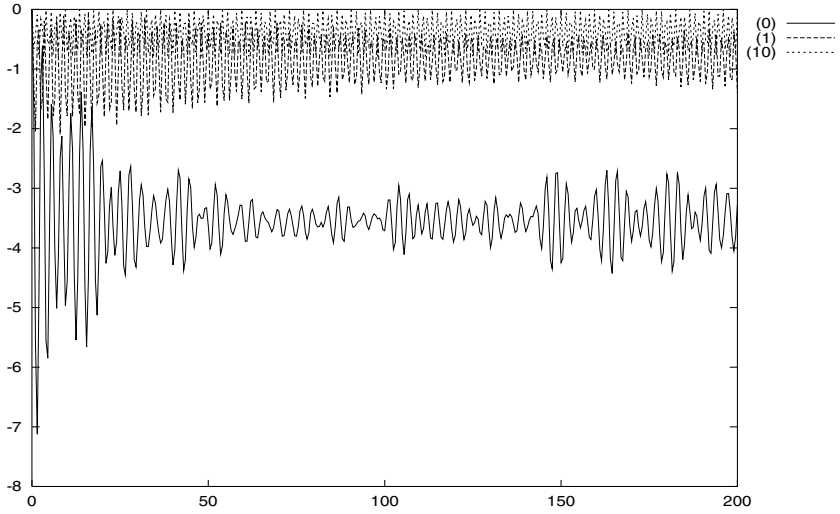

Figure 12. Thermal average $\langle H_I \rangle$ of the interaction Hamiltonian versus $\omega_c t$ (baths of 11 spins).

Table 1. $\langle \Sigma_x \rangle|_{\lambda=10}$ as a function of N.

Number of bath spins	$\langle \Sigma_x \rangle$ for $\lambda = 10$
7	−0.011 147
9	−0.006 724
11	−0.004 967

Comparing equation (26) with equation (27) shows that $\langle \Sigma_x \rangle$ is a decreasing function of λ for baths of both even and odd numbers of spins but $\langle \Sigma_x \rangle$ for $\lambda = 10$ is two orders of magnitude larger for the 11-spin bath than for the 10-spin bath. Table 1 shows that as N increases $\langle \Sigma_x \rangle$ (for $\lambda = 10$) decreases. The even–odd difference is thus a finite-size effect which should vanish in the thermodynamic limit.

4.2. Ferromagnetic interactions

The entropy for the ferromagnetic case is shown in figure 13. The data were obtained for a bath of 10 spins; we use a semi-logarithmic scale to distinguish the curve for $\lambda = -2$ from the x-axis. We do not show data for values of $\lambda < -2$ because they overlap. The behaviour of the entropy is similar in the ferromagnetic and antiferromagnetic cases; the only significant difference is that in the ferromagnetic case a suppression of the entropy can be achieved with weaker intra-environmental interactions.

The most relevant difference between antiferromagnetic and ferromagnetic baths emerges when one considers the behaviour of the polarization vector (19) shown in figures 14–16. We have chosen a timescale appropriate to the fast oscillations of the polarization components (but long enough to be representative of the long-time behaviour of $\vec{P}(t)$). For $\lambda \leqslant -2$ the components of the polarization vector assume a strongly oscillatory behaviour. This is consistent with the suppression of entropy since entropy depends only on the norm of the polarization vector which can stay close to unity even if individual components of $\vec{P}$ oscillate in time. Such polarization dynamics, however, is very different from that observed in the

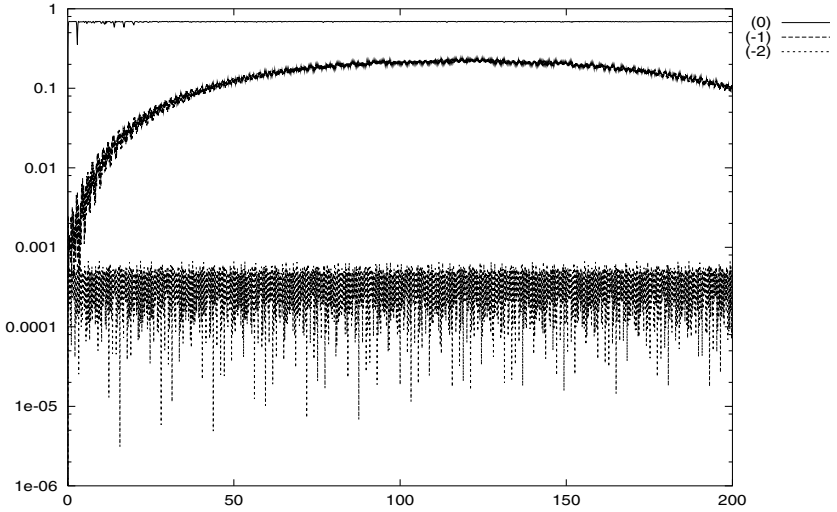

Figure 13. $\ln(S_0)$ versus $\omega_c t$ (10 spin bath).

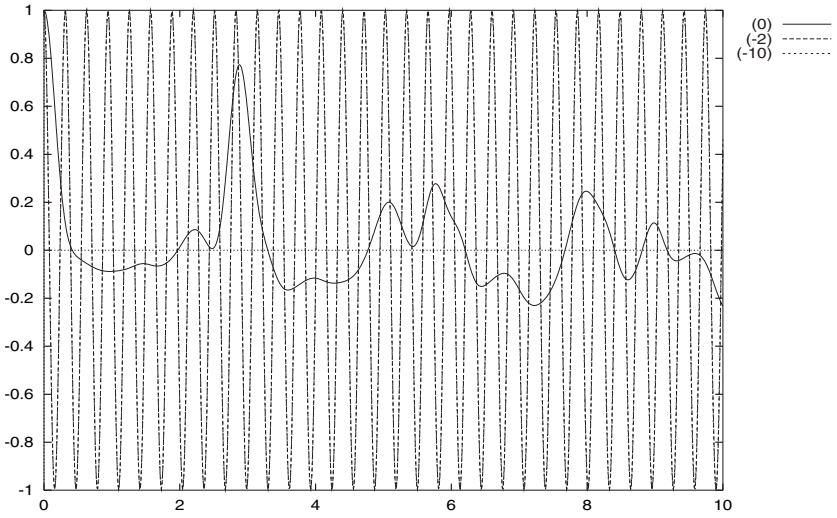

Figure 14. P_z versus $\omega_c t$ (10 spin bath).

antiferromagnetic case where $P_z(t) \simeq 1$ and $P_x(t) \simeq P_y(t) \simeq 0$ at all times. Term (21) is not negligible for ferromagnetic interactions, as can be seen in figure 17, where we represent the thermal average of the interaction Hamiltonian as a function of time. For $\lambda \leqslant -2$, the interaction term $\langle H_I(t)\rangle$ becomes almost independent of the strength of the spin–spin coupling and oscillates around a non-zero value.

This behaviour can be explained by writing the bath Hamiltonian in the form (23) and by observing that in the limit of strong ferromagnetic interaction

$$H_B = -\frac{|\lambda|}{2}\big[\Sigma_x^2 - N\mathbf{1}\big] + O(\lambda^0). \tag{28}$$

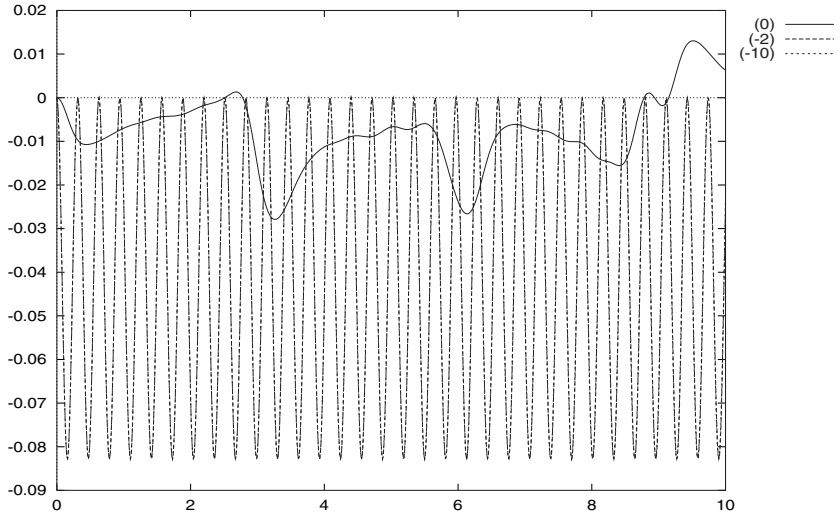

Figure 15. P_x versus $\omega_c t$ (10 spin bath).

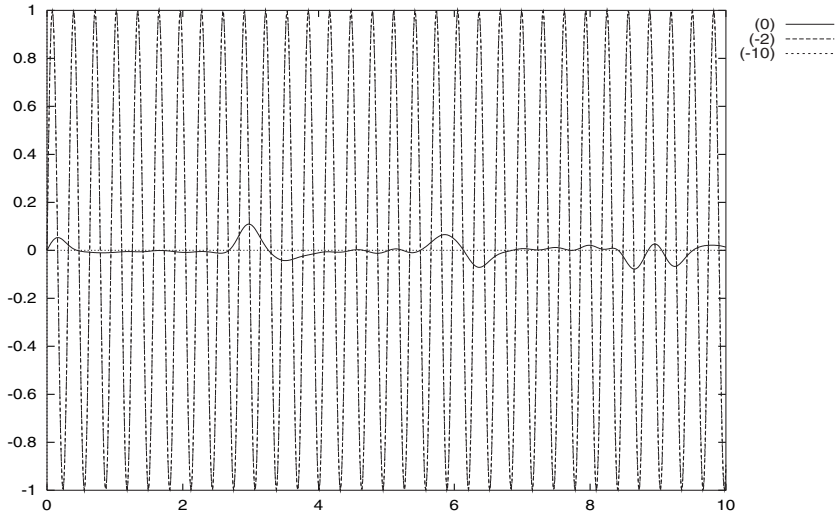

Figure 16. P_y versus $\omega_c t$ (10 spin bath).

Note that the antiferromagnetic and ferromagnetic Hamiltonians (24) and (28) are identical but with opposite sign. The bath eigenstates of lowest energy are eigenstates of Σ_x in both cases, but with $\langle\phi_n^B|\Sigma_x|\phi_n^B\rangle \simeq 0$ in the antiferromagnetic case and $|\langle\phi_n^B|\Sigma_x|\phi_n^B\rangle| \gg 1$ in the ferromagnetic case. This is confirmed by figure 18, which represents $\langle\phi_n^B|\Sigma_x|\phi_n^B\rangle$ as a function of the index n. Not surprisingly, the distribution of points for $\lambda = -10$ is almost the reverse of the distribution for $\lambda = 10$ shown in the corresponding figure 7. Consequently, the coupling term (21) is significantly larger for a ferromagnetic bath than it is for a antiferromagnetic one. Thus, diagonal matrix elements of the coupling operator Σ_x are large while off-diagonal matrix elements are again zero.

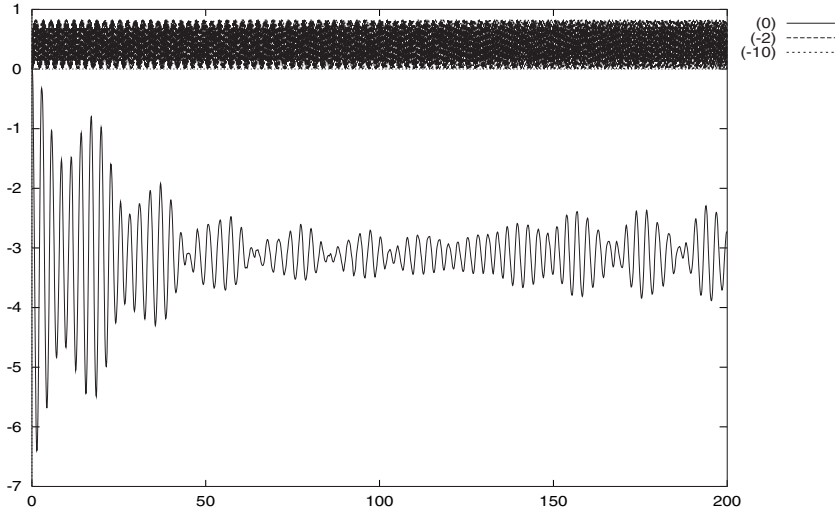

Figure 17. $\langle H_I \rangle$ versus $\omega_c t$ (10 spin bath).

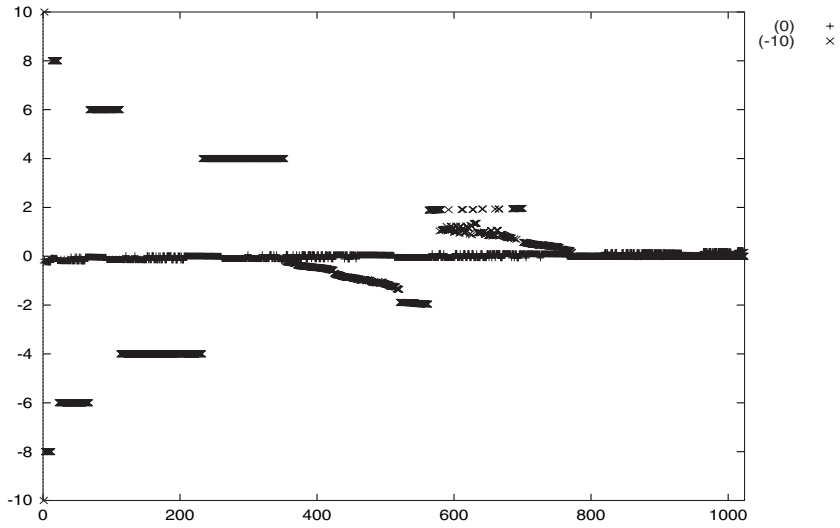

Figure 18. Expectation value $\langle \phi_n^{(B)} | \Sigma_x | \phi_n^{(B)} \rangle$ versus n for $\lambda = 0$ and $\lambda = -10$ (10 spin bath).

It is important to note that the oscillations of the average interaction Hamiltonian (21) are synchronous with those of $P_x(t)$: more precisely

$$\beta'(t) = \langle H_I(t) \rangle / P_x(t)$$

is practically constant in time and, for $\lambda \leqslant -2$, it takes the value

$$\beta' \simeq -10$$

regardless of the strength of the spin–spin coupling. The value of β' is easily explained. The matrix element $\langle \phi_1^B | \Sigma_x | \phi_1^B \rangle$ corresponding to the lowest energy bath eigenstate is -10 while that of the next lowest is 10. However, the energy gap between these states is 0.2 leading to a population ratio $p_2/p_1 \sim 10^{-5}$ at $kT = 0.02$. Hence, the lowest energy state is the only one

populated (in sharp contrast to the antiferromagnetic case) and its Σ_x eigenvalue is -10. This also explains why decoherence is more easily suppressed in the ferromagnetic case.

Thus the central spin interacts with the bath through

$$H_I^{\text{eff}} = \beta' \sigma_x^{(0)} \tag{29}$$

and the evolution of the central spin is dictated by Hamiltonian (4) with a renormalized β parameter:

$$\beta \to \tilde{\beta} = \beta + \beta' \simeq -10. \tag{30}$$

Solving the Heisenberg equations for the renormalized central spin with initial conditions $P_z(0) = 1$, $P_x(0) = P_y(0) = 0$ gives

$$\begin{aligned} P_x(t) &= \frac{2\tilde{\beta}\omega_0}{\Omega^2}(1 - \cos\Omega t) \\ P_y(t) &= -\frac{2\tilde{\beta}}{\Omega}\sin\Omega t \\ P_z(t) &= 1 - \frac{4\tilde{\beta}^2}{\Omega^2}(1 - \cos\Omega t) \end{aligned} \tag{31}$$

where $\Omega = \sqrt{\omega_0^2 + 4\tilde{\beta}^2}$. Comparing equation (31) with the actual data shows that (29) is correct. Figures 14–16 do not show $\vec{P}(t)$ predicted by equation (31) because of overlapping of the various curves.

We therefore conclude that the only effect that a low-temperature bath with internal ferromagnetic interactions has on the central spin is a renormalization (30) of the β parameter in the Hamiltonian (4) (i.e., a Lamb shift). In both the antiferromagnetic and the ferromagnetic cases, therefore, when intra-environmental interactions are strong the dynamics of the central spin is almost autonomous from that of the bath and is dictated by a Hamiltonian of the form (4).

As a last remark on the ferromagnetic case, we observe that the dynamics of the central spin is unaffected by whether the bath is composed of an even or odd number of spins.

5. Discussion and conclusions

In this work we considered a spin-1/2 subsystem coupled to a low-temperature bath of interacting spin-1/2 modes. We focussed our attention on the effects of antiferromagnetic and ferromagnetic intra-environmental interactions on decoherence. In both cases strong intra-environmental interactions suppress decoherence by making the dynamics of the central spin almost autonomous from the bath itself. More precisely, strong antiferromagnetic couplings among bath spins make the average value of the subsystem-environment interaction Hamiltonian vanish, thereby making the central spin evolve with its unperturbed and uncoupled Hamiltonian. Strong ferromagnetic couplings among bath spins, on the other hand, cause a Lamb shift of the subsystem Hamiltonian but otherwise leave it to evolve in isolation.

These effects can be schematically explained by considering Hamiltonian (3) with $H_I = SB$ where S and B are subsystem and bath operators. Now, the eigenstates of H_B are also eigenstates of B for strong intra-environmental coupling in our model. Hence the off-diagonal matrix elements of B in this eigenbasis are zero and so (3) cannot couple bath eigenstates. Since the initial states of the full system are proportional to bath eigenstates for initial conditions (13), it follows that the time evolved reduced density must be of the form

$$\rho_0(t) = \sum_n \frac{\mathrm{e}^{-E_n/kT}}{Q}\, \mathrm{e}^{-\mathrm{i}(H_0 + SB_n)t}\, \rho_0(0)\, \mathrm{e}^{\mathrm{i}(H_0 + SB_n)t} \tag{32}$$

where B_n is the eigenvalue of B corresponding to eigenstate $\left|\phi_n^{(B)}\right\rangle$ of H_B. In the antiferromagnetic case we found that all relevant B_n were zero for strong intra-environmental coupling and hence the dynamics was free of decoherence. For the ferromagnetic case we found that only the lowest energy state was populated at low temperature and so only one term contributes to (32) and again the dynamics is coherent, but with a Lamb shift.

We expect similar effects to occur in more general baths of coupled anharmonic oscillators. The key issue as we have seen is what happens to the matrix elements of the spin-bath coupling Hamiltonian, in the eigenbasis of the bath, when bath self-interactions are turned on. To suppress decoherence the off-diagonal matrix elements must be small. Clearly in an integrable bath (i.e., no self-interaction) some off-diagonal matrix elements will be large due to selection rules. One would thus expect strong decoherence for integrable environments. In the case of chaotic environments it is known that the off-diagonal matrix elements are of order $h^{(N-1)/2}$ smaller than the diagonal matrix elements [37–39], where N is the number of environmental modes. Specifically, the diagonal matrix element of a subsystem-environment coupling operator B,

$$B_n = \langle n|B|n\rangle \simeq \frac{\int \mathrm{d}\mathbf{x}\, \delta(E_n - H(\mathbf{x}))B(\mathbf{x})}{\int \mathrm{d}\mathbf{x}\, \delta(E_n - H(\mathbf{x}))} = \langle B\rangle \tag{33}$$

is its microcanonical average at energy $E = E_n$. Here $\mathbf{x}$ represents the $6N$ momenta and coordinates of the environment and $B(\mathbf{x})$ represents the Wigner function of B. Similarly [38, 39],

$$|\langle n|B|m\rangle|^2 \simeq h^{N-1} \frac{\int_{-\infty}^{\infty} \mathrm{d}t \langle [B(0) - \langle B\rangle][B(t) - \langle B\rangle]\rangle \exp[\mathrm{i}(\bar{E}_n - \bar{E}_m)t/\hbar]}{\int \mathrm{d}\mathbf{x}\delta((\bar{E}_n + \bar{E}_m)/2 - \bar{H}(\mathbf{x}))} \tag{34}$$

where the microcanonical averages are evaluated at energy $(\bar{E}_n + \bar{E}_m)/2$. Note that the energies which appear in equation (34) are the unfolded energies $\bar{E}_n = N(E_n)$, where $N(E)$ is the average number of levels with energy less than E_n, rather than the energies E_n themselves. This is so because the off-diagonal matrix elements of B can be written in the form (34) only if the average spacing between energy levels is constant.

The time correlation function in equation (34) decays exponentially at short time as $\exp(-\Omega^2 t^2)$ where Ω is its spectral width. Hence equation (34) gives a result

$$|\langle n|B|m\rangle|^2 \propto h^{N-1} \exp[-(\bar{E}_n - \bar{E}_m)^2/4\Omega^2\hbar^2]. \tag{35}$$

In figure 19 we plot the logarithm of the squared off-diagonal matrix elements of $B = \Sigma_x$ for the spin-bath Hamiltonian (5) (for $N = 14$ and $\lambda = 10$ with antiferromagnetic interaction) against the squared difference in energy and obtain a plot which exhibits an average linear behaviour in agreement with equation (35).

Since Planck's constant is small and N is very large, the off-diagonal matrix elements (35) for a chaotic environment are negligible. Therefore, we expect at most a Lamb shift of the subsystem for each eigenstate of the bath and hence a reduced density like (32).

However, the Lamb shifts can vary from state to state and hence still cause decoherence [4]. If the coupling operator B is proportional to the coordinates of the bath, then scaling the momenta and coordinates of the bath as $\mathbf{x} = \sqrt{E_n - E_1}\,\tilde{\mathbf{x}}$ in equation (33) gives $B_n = \sqrt{E_n - E_1}F(\sqrt{E_n - E_1})$ where $F(z)$ is a function which can be expanded in powers of z and E_1 denotes the ground energy of the bath. The order z^0 term vanishes by symmetry and so

$$B_n = b(E_n - E_1) + \cdots \tag{36}$$

where b is independent of E_n. Figure 20 shows the diagonal matrix elements of $B = \Sigma_x$ for the spin-bath Hamiltonian (5) plotted against E_n. In the figure, we plot the data relative to the

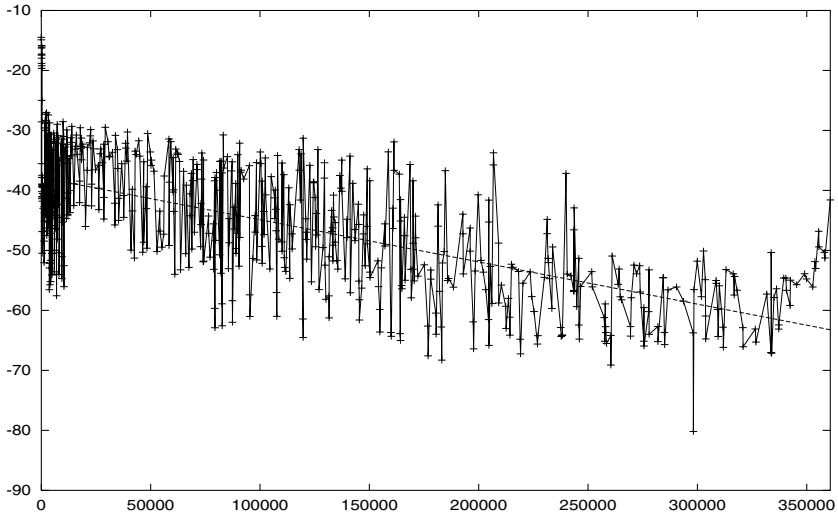

Figure 19. $\ln(\langle\phi_1^{(B)}|\Sigma_x|\phi_n^{(B)}\rangle^2)$ versus $(\bar{E}_1 - \bar{E}_n)^2$, with n ranging over the first 600 energy levels ($\lambda = 10$, 14 spin bath). The straight line is a fit to the data.

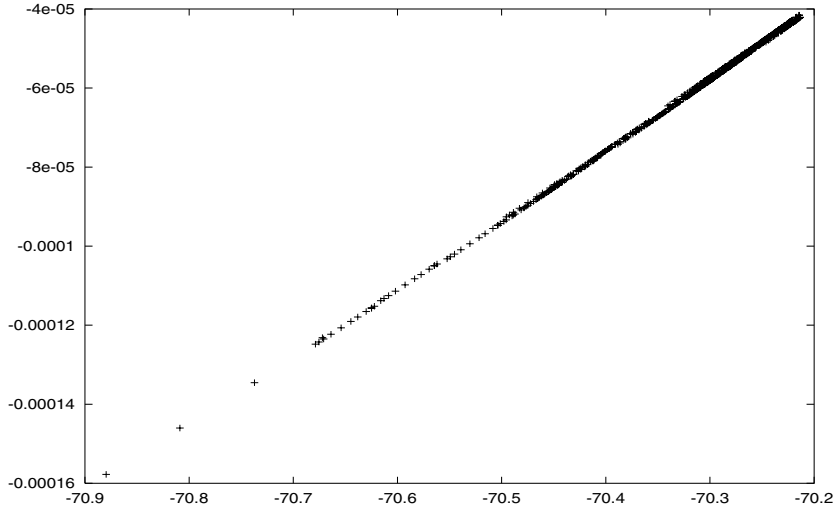

Figure 20. $\langle\phi_n^{(B)}|\Sigma_x|\phi_n^{(B)}\rangle$ versus E_n ($\lambda = 10$, 14 spin bath; data relative to the 600 bath eigenstates of lowest energy).

low-energy part of the bath spectrum; again we see the predicted linear dependence. Thus, for sufficiently low energies and large intra-environmental coupling

$$B_n/\hbar\omega_0 = b(E_n - E_1)/\hbar\omega_0 \ll 1 \qquad B_n/\lambda = b(E_n - E_1)/\lambda \ll 1$$

and so there is always a low-energy region where the diagonal matrix elements are practically constant. Hence, decoherence should be negligible for chaotic baths at low temperatures.

In the specific case of He in silicon or diamond $b \sim 10^{-4}$ and decoherence should be suppressed even at high temperature. There are well-known [31] optical transitions for interstitial He in Si with $\hbar\omega_0 \sim 1$ eV. Assuming that an electric-dipole forbidden state can be found with comparable energy and assuming that only bath states with energies less than

0.05 eV contribute at liquid nitrogen temperatures (i.e. $kT = 0.007$ eV), then $B_n/\hbar\omega_0 \sim 10^{-5}$. Similarly, $\lambda \sim 0.005$ eV [32] and so $B_n/\lambda \sim 10^{-3}$. Hence, decoherence of He in Si should be minimal even at 77 K. We expect even less decoherence for diamond for which $\lambda \sim 0.03$ eV [32].

We think it is appropriate to conclude this paper with a brief remark on the limitations of the present analysis. Although the general arguments presented in this section suggest that chaotic baths should cause less decoherence than baths with regular dynamics, we recognize that our semiclassical argument does not constitute a rigorous proof and that further investigation is necessary in order to clarify the links between chaos and decoherence. More work is also required to reach a complete understanding of the realistic model (1) for which the spin model (3) can provide only a somewhat crude approximation. We think that these shortcomings can be at least partially overcome by considering a bath composed of nonlinearly coupled oscillators; the study of such a system will be the object of future work.

Acknowledgment

The authors gratefully acknowledge the financial support of the Natural Sciences and Engineering Research Council of Canada.

References

[1] Caldeira A O and Legget A J 1983 *Ann. Phys., NY* **149** 374
[2] Weiss U 1999 *Quantum Dissipative Systems* 2nd edn (Singapore: World Scientific)
Leggett A J, Chakravarty S, Dorsey A T, Fisher M P A, Garg A and Zwerger W 1987 *Rev. Mod. Phys.* **59** 1
[3] Haake F and Reibold R 1985 *Phys. Rev.* A **32** 2462
[4] See Prokof'ev N V and Stamp P C E 2000 *Rep. Prog. Phys.* **63** 669, and references therein
[5] Alicki R 2002 *Preprint* quant-ph/0205173
Alicki R 1991 *J. Phys. A: Math. Gen.* **24** 4743
[6] Zurek W H 2001 *Nature* **412** 712
[7] Braun D, Haake F and Strunz W T 2001 *Phys. Rev. Lett.* **86** 2913
[8] Arnold V I and Avez A 1989 *Ergodic Problems of Classical Mechanics* (New York: Addison-Wesley)
[9] Haake F 2001 *Quantum Signatures of Chaos* 2nd edn (Berlin: Springer)
Berry M V 1983 *Chaotic Behavior in Quantum Systems* ed G Ioos, R H G Helleman and R Stora (Amsterdam: North-Holland)
[10] Berry M V 1989 *Proc. R. Soc.* A **423** 219
[11] Wilkie J and Brumer P 1997 *J. Chem. Phys.* **107** 4893
Wilkie J and Brumer P 1991 *Phys. Rev. Lett.* **67** 1185
[12] Gaspard P, Briggs M E, Francis M K, Sengers J V, Gammon R W, Dorfmann J R and Calabrese R V 1998 *Nature* **394** 865
[13] Miyano T, Munetoh S, Moriguchi K and Shintani A 2001 *Phys. Rev.* E **64** 016202
[14] Mucciolo E R, Capaz R B, Altshuler B L and Joannopoulos J D 1994 *Phys. Rev.* B **50** 8245
[15] Maris H J and Tamura S 1993 *Phys. Rev.* B **47** 727
Shields J A, Msall M E, Carroll M S and Wolfe J P 1993 *Phys. Rev.* B **47** 12510
[16] Lo H-K, Popescu S and Spiller T 1998 *Introduction to Quantum Computation and Information* (Singapore: World Scientific)
[17] Brumer P and Shapiro M 1998 *Laser Part. Beams* **16** 599
[18] Mujica V, Nitzan A, Mao Y, Davis W, Kemp M, Roitberg A and Ratner M A 1999 *Adv. Chem. Phys.* **107** 403
[19] Gulde S, Riebe M, Lancaster G P T, Becher C, Eschner J, Häffner H, Schmidt-Kaler F, Chuang I L and Blatt R 2003 *Nature* **421** 48
[20] See for example Cirac J I and Zoller P 200 *Nature* **404** 579
Cirac J I and Zoller P 1995 *Phys. Rev. Lett.* **74** 4091
[21] Barenco A, Deutsch D, Ekert A and Jozsa R 1995 *Phys. Rev. Lett.* **74** 4083
[22] Berman G P, Doolen G D and Tsifrinovich V I 2000 *Superlattices Microstruct.* **27** 89

[23] Zanardi P and Rasetti M 1997 *Phys. Rev. Lett.* **79** 3306
Knill E, Laflamme R and Viola L 2000 *Phys. Rev. Lett.* **84** 2525
Kempe J, Bacon D, Lidar D A and Whaley K B 2001 *Phys. Rev.* A **63** 042307
[24] Feynman R P and Vernon F L Jr 1963 *Ann. Phys., NY* **24** 118
[25] Nakajima S 1958 *Prog. Theor. Phys.* **20** 948
Zwanzig R 1960 *J. Chem. Phys.* **33** 1338
Zwanzig R 1961 *Lectures in Theoretical Physics* vol 3 (New York: Interscience)
[26] Gaspard P and Nagaoka M 1999 *J. Chem. Phys.* **111** 5668
Suárez A, Silbey R and Oppenheim I 1992 *J. Chem. Phys.* **97** 5101
Romero-Rochin V and Oppenheim I 1988 *J. Stat. Phys.* **53** 307
Romero-Rochin V and Oppenheim I 1989 *Physica* A **155** 52
Romero-Rochin V, Orsky A and Oppenheim I 1989 *Physica* A **156** 244
Redfield A G 1965 *Adv. Magn. Reson.* **1** 1
[27] Wilkie J 2001 *J. Chem. Phys.* **115** 10335
Wilkie J 2001 *J. Chem. Phys.* **114** 7736
Wilkie J 2000 *Phys. Rev.* E **62** 8808
[28] See for example Wang H, Thoss M and Miller W H 2001 *J. Chem. Phys.* **115** 2991
[29] Davies G 1981 *Rep. Prog. Phys.* **44** 787
[30] Chacham H, Alves J Y A, de Siqueria M L and Leite J R 1986 *Int. J. Quant. Chem.* **20** 347
[31] Estreicher S K, Weber J, Derecskei-Kovacs A and Marynick D S 1997 *Phys. Rev.* B **55** 5037
[32] Anastassakis E, Cantarero A and Cardona M 1990 *Phys. Rev.* B **41** 7529
[33] Makri N 1999 *J. Chem. Phys.* **111** 6164
Shao J S and Hanggi P 1998 *Phys. Rev. Lett.* **81** 5710
[34] Dube M and Stamp P C E 2001 *Chem. Phys.* **268** 257
[35] Press W H, Teukoslky S A, Vetterling W T and Flannery B P 1992 *Numerical Recipes in Fortran 77* 2nd edn (Cambridge: Cambridge University Press)
[36] DOP853.f Hairer E and Wanner G http://elib zib de/pub/elib/hairer-wanner/nonstiff/
[37] Pechukas P 1983 *Phys. Rev. Lett.* **51** 943
[38] Feingold M and Peres A 1986 *Phys. Rev.* A **34** 591
[39] Wilkie J and Brumer P 1997 *Phys. Rev.* A **55** 43